Physica E 84 (2016) 324–329

Contents lists available at ScienceDirect

Physica E

journal homepage: www.elsevier.com/locate/physe

Coulomb screening effects on the optoelectronic far-infrared properties of spatially separated few-layer graphene

C.H. Yang [a,*], P. Wan [a], Q.F. Li [a], Z.M. Ao [b,*]

[a] School of Physics and Optoelectronic Engineering, Nanjing University of Information Science and Technology, Nanjing 210044, China
[b] Institute of Environmental Health and Pollution Control, School of Environmental Science and Engineering, Guangdong University of Technology, Guangzhou 510006, China

HIGHLIGHTS

- The optical transitions in layer structures with isolated mono- or bilayer graphene.
- The positions of the transition turning points can be tuned.
- The system and structure parameters can be determined from the optical conductivity.
- One observed peak in the infrared region with the interlayer screened effect.

ARTICLE INFO

Article history:
Received 10 June 2016
Received in revised form
4 August 2016
Accepted 4 August 2016
Available online 5 August 2016

Keywords:
Few-layer graphene
Optoelectronic property
Screening effect

ABSTRACT

We investigate the longitudinal optical conductivity of spatially separated few-layer graphene analytically and numerically. Each layer could be monolayer or bilayer graphene. The density–density correlation function has been screened by the dielectric function using the random phase approximation, which includes the inter-layer Coulomb coupling. In the presence of the potential function between the layers, the carrier densities in each layer can be tuned respectively. In these two-dimensional layered structures, the main contributions to the optical conductivity are from the intra- and inter-band transition channels in a same layer. In the infrared region, the Drude optical conductivity was observed by the unscreened intra-band transition process. But in the presence of the inter-layer Coulomb interaction, one peak structure of the optical conductivity is observed which can be modified by the dielectric environment. From the number of turning points and the turning positions, the carrier density, the Fermi wavevector, and the layered structure can be determined.

1. Introduction

Graphene, single atomic layer thickness, was fabricated experimentally by Geim et. al [1]. This ultra-thin material exhibits very exceptional and excellent physical properties, such as, Klein tunning [2], high mobilities [3], unique quantum Hall effect [1], and so on. Using the applied field (or gate voltage), the carrier density can be tuned [4–6] and the corresponding transport properties can be measured experimentally. For example, using the global gate and a metallic top gate in single layer graphene, which led to the electrostatic potential barrier, n–p junctions with tunable charge densities can be obtained and the transport measurements in the presence of barrier can be performed experimentally [7–9]. In the presence of the barrier structure, the charge transmission coefficient depends on the height and the width of the barrier and the transmittance value is less than 1. But for graphene material, owing to the suppression of backscattering [10,11], the charge exhibits perfect transmission through the barrier at normal incidence regardless of the barrier characteristics. During the fabrication of graphene material, the number of graphene layer has many possibilities, such as, monolayer, bilayer, and few layers. In a more than one layer system with top and back gates, the out-of-plane electric field creates a different potential between the layers [12] and the carrier densities (doping level) in both layers can be independently controlled by double gates [4,5,13,14]. The carrier density in each layer can be obtained by the capacitance between graphene and the gates [13]. Seyong Kim et al. used an ultrathin dielectric layer to separate the bilayer graphene into two independently contacted graphene single layers [4]. The dependence of the layer resistivities on the back gate bias indicates that the charge densities in both top and bottom

* Corresponding authors.
E-mail addresses: yangcuihong1978@163.com (C.H. Yang), Zhimin.Ao@uts.edu.au (Z.M. Ao).

http://dx.doi.org/10.1016/j.physe.2016.08.008
1386-9477/

graphene layers are induced differently with the applied back gate voltage. At the Fermi energy, the kinetic energy in a different layer is different. Khrapach et al. intercalated the $FeCl_3$ into two- to five-layer graphene [14]. The Raman spectra measurements indicate the decoupling of the few layer graphene. The longitudinal magneto-conductance oscillates as a function of perpendicular magnetic field at $T < 10$ K, which indicates the distinct charge densities in different layers. From the Hall resistance measurement, it has found that the monolayer and bilayer graphene are included in the intercalation graphene system. The optical transmission in the visible wavelength range slightly decreases at low wavelength. Bao et al. demonstrated an increase of optical transmittance in the visible range upon Lithium intercalation for 3–60 graphene layers, which is explained by the suppression of interband transitions [15]. As for the double layer systems, drag conductivity is always employed to investigate the intra- and inter-layer interactions [4,16–18]. Min et al. calculated the static polarizability and screening of multilayer graphene which is dependent on the layer number and includes the intra- and interband polarizability [19]. The theoretical Thomas-Fermi screening wave vector results show different behaviors for several stacking sequences which implies the importance of the layer structure (see Figs. 1(a) and (b) in Ref. [19]). Das Sarma et al. investigated the intrinsic and extrinsic plasmons for single and double-layer systems and the effects of the layered structure, electron densities, the background lattice dielectric constant, and the temperature are included in their investigations [20–22]. In Ref. [21], the structures for monolayer graphene (MLG), bilayer graphene (BLG), double-layer MLG, and double layer BLG are designed to investigate the plasmon properties.

The optical conductivity in graphene also exhibits other important properties with inter- and intra-band transitions channels which has been widely investigated experimentally [23–25]. The experimental value of the optical conductivity per graphene layer (or an optical sheet conductivity) is almost a constant and close to $e^2/(4\hbar)$ above two times the Fermi energy ($2E_F$), which is independent from the frequency and the inter-layer hopping. In the far-infrared region, the Drude optical conductivity $4 \sim 100e^2/(4\hbar)$ was observed accompanied by the intra-band transition contribution. Another observation is that the optical sheet conductivity showed a threshold structure at $2E_F$ and the turning points (or the Fermi energy E_F) can be tuned by the gate voltage. Theoretically, the Boltzmann transport theory and/or the Kubo formula were employed to investigate the optical conductivity as a function of the gate voltage and the optical frequency with the disorder broadening from impurity and phonon scattering [26–33]. The optical conductivity is proportional to the layer number multiplying the universal optical conductivity [31]. Taking into account of the full energy dispersion, the results for the optical conductivity from the infrared to the ultraviolet frequency regions are obtained with extra peak structures observed [33].

In this paper, several isolated parallel two dimension (2D) graphene are separated by a distance d with an ultrathin dielectric layer. The interlayer distance with the intercalation dielectric layer is larger than the distance where the out-of-plane π orbits from two adjacent graphene sheets overlap ($d \sim 3.5$ Å). The difference between the isolated paralled 2D material and bilayer or trilayer material is that there is no interlayer tunneling, instead of the interlayer Coulomb interaction. The dielectric function was employed to investigate the longitudinal optical conductivity theoretically in these systems. The dependence on the layer number, charge density, dielectric environment, Coulomb interaction is analyzed detailed. Here, we refer to the electron systems (i.e., extrinsic graphene systems) where the Fermi energy $E_F > 0$.

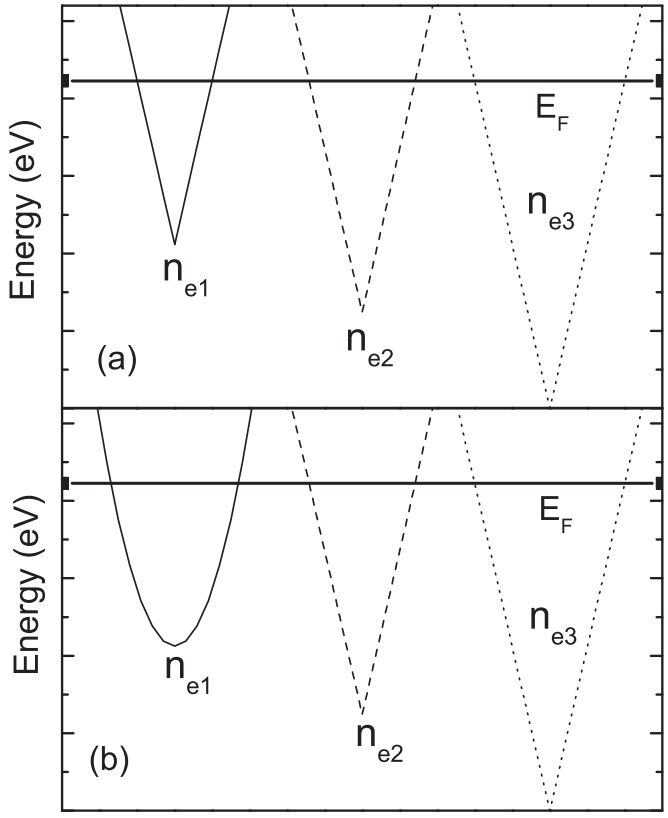

Fig. 1. Schematic of the energy structure for three layer graphene system.

2. Theoretical approaches

For a several layer system, using the mean-field random phase approximation, the dielectric tensor $\varepsilon_{l,m}$, where $l, m = 1, 2, \cdots$ denoting the different layer, can be obtained as [20,34]

$$\varepsilon_{l.m}(q, \omega) = \delta_{l,m} - V_{l,m}\Pi_m(q, \omega). \quad (1)$$

Here, $\Pi_m(q, \omega)$ is the density–density (d–d) correlation function. $V_{l,m}$ are the intra-layer ($l=m$) and inter-layer ($l \neq m$) Coulomb interaction matrix elements. The d–d correlation function for mono- and bilayer graphene can be obtained as $\Pi_m(\omega, q) = g_s g_v \sum_{s,s',\mathbf{k_m}} \frac{1+ss'A_{k_mq}}{2} \frac{f_{s,\mathbf{k_m}} - f_{s',\mathbf{k_m+q}}}{\hbar\omega + E_{s,\mathbf{k_m}} - E_{s',|\mathbf{k_m+q}|} + i\Gamma_m}$ [35–37]. $g_s=2$ is spin degeneracy. There are two points K and K' at the corner of the graphene Brillouin zone, called the Dirac points. $g_v=2$ refers to this degeneracy. $f_{s,\mathbf{k_m}}$ is the Fermi-Dirac distribution function in the m^{th} layer. $s, s' = \pm 1$ refers to the conduction band (+ 1) and the valence band (− 1). $(1 + ss'A_{k_mq})/2$ comes from the overlap of carrier states. $A_{k_mq} = \cos\varphi_m$ and $A_{k_mq} = \cos 2\varphi_m$ in monolayer and bilayer graphene respectively, with $\cos\varphi_m = (k_m + q\cos\theta_m)/|\mathbf{k_m} + \mathbf{q}|$, θ_m being the angle between $\mathbf{k_m}$ and $\mathbf{q}$, $\mathbf{k'_m} = \mathbf{k_m} + \mathbf{q}$. In monolayer graphene, $E_{s,k} = s\hbar v_F|\mathbf{k}|$ (v_F being the Fermi velocity of graphene). In bilayer graphene, $E_{s,\mathbf{k}} = s\hbar^2k^2/(2\,\mathrm{m})$, $m \approx 0.033m_e$ is the effective mass of bilayer graphene with m_e being the free-electron mass. Coulomb interactions between each layer make the isolated layer into a system. $V_{l,l} = v_q = 2\pi e^2/(\kappa q)$ is the intra-layer Coulomb interaction. κ is the static dielectric constant for graphene. $V_{l,m} = e^{-qd|l-m|}v_q$ is the inter-layer Coulomb interaction with d being the distance between the adjacent layers. Γ_m is the broadening width induced by the carrier scattering process.

The longitudinal optical conductivity can be obtained by the dielectric function [38,39]

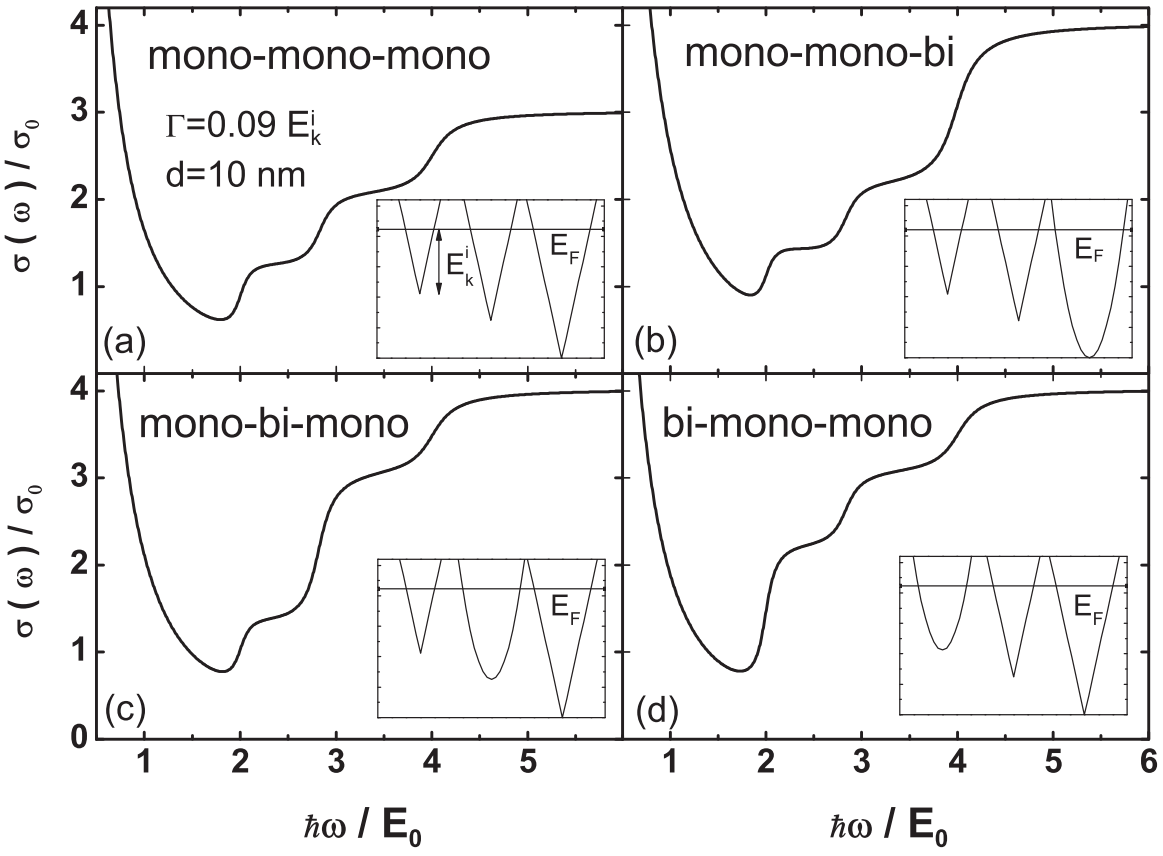

Fig. 2. The optical conductivity as a function of photon energy for fixed electron densities n_{e1}, n_{e2}, n_{e3} in a three layer system. (a) indicates the case that each layer is monolayer graphene. The structures in (b)–(d) are only one monolayer graphene layer replaced by a bilayer graphene layer which can be seen in the inset of the figures. $d=10$ nm is the distance between the layers. $\sigma_0=\frac{e^2}{4\hbar}$, $\kappa=2.5$.

$$\sigma_{xx}(\omega)=-e^2\omega\lim_{q\to 0}\frac{1}{q^2}\sum_m \mathrm{Im}\frac{\Pi_m(q,\omega)}{\varepsilon(q,\omega)}. \tag{2}$$

$\varepsilon(q,\omega)$ is the determination of the dielectric matrix function. ω is the frequency of the incident light. $q\to 0$ reflects a fact that the electron-photon scattering does not change the wavevector of an electron. The optical conductivity is related to the imaginary part of the dielectric function, which can be understood from Maxwell equations with a complex dielectric function $\varepsilon'=\varepsilon+i\sigma/\omega$ being introduced to investigate the optical absorption problems. The longitudinal optical conductivity $\sigma_{xx}(\omega)$ is proportional to $(\mathrm{Im}\Pi\cdot\mathrm{Re}\varepsilon-\mathrm{Re}\Pi\cdot\mathrm{Im}\varepsilon)$. The intra- and inter-band d–d correlation functions contribute to the real and imaginary parts. The real parts in the i^{th} layer are $\mathrm{Re}\Pi^{+}_{L,i}(q,\omega)=L\frac{g_s g_v E_F^i q^2}{4\pi(\hbar\omega)^2}\frac{1-x_i^2}{(1+x_i^2)^2}$, and $\mathrm{Re}\Pi^{-,+}_{L,i}\left(q,\omega\right)=L\frac{g_s g_v q^2}{16\pi}\left[\frac{\hbar\omega}{2A_i}\ln\frac{k^{2L}}{R_i}+\left(\frac{(\hbar\omega)^2}{A_i}-1\right)\frac{1}{\Gamma_i}\arctan\frac{\Delta}{\Gamma_i}\right]_{k_F^i}^{k_c}$. The imaginary parts are $\mathrm{Im}\Pi^{+}_{L,i}(q,\omega)=-L\frac{g_s g_v q^2 E_F^i\Gamma_i}{2\pi(\hbar\omega)^3}$, and $\mathrm{Im}\Pi^{-,+}_{L,i}\left(q,\omega\right)=-L\frac{g_s g_v q^2\Gamma_i}{16\pi A_i}\left[\frac{1}{2}\ln\frac{k^{2L}}{R_i}+\frac{\hbar\omega}{\Gamma_i}\arctan\frac{\Delta}{\Gamma_i}\right]_{k_F^i}^{k_c}$. Here, $L=1, 2$ is for monolayer and bilayer graphene, respectively. This coefficient is similar to the obtained plasmon results in MLG and BLG. These two plasmon analytical results are identical except for an extra factor of $\sqrt{2}$ in the BLG case from the Table I in Ref. [21]. $x_i=\frac{\Gamma_i}{\hbar\omega}$, $\Delta=2\gamma k-\hbar\omega$, $\hbar^2k^2/(m)-\hbar\omega$ for monolayer and bilayer graphene, respectively. $A_i=(\hbar\omega)^2+\Gamma_i^2$, $R_i=\Delta^2+\Gamma_i^2$, $\gamma=\hbar v_F$ and k_c is the cutoff wave vector above which the linear energy dispersion approximation breaks down for graphene, $k_c\sim 1/a$ (a being the distance between C–C bond). The real and imaginary parts of intra- or inter-band d–d correlation function have much common factors, and have similar relationship to the broadening width, Fermi energy, q-wave vector, and the optical frequency.

For a few layer system, the inter-layer coupling gives the extra contributes to the dielectric function. For example, The determination of the dielectric function for three layers can be obtained

$$\begin{aligned}\varepsilon_3(q,\omega)=1&-v_q[\Pi_1(q,\omega)+\mathrm{Im}\Pi_2(q,\omega)+\mathrm{Im}\Pi_3(q,\omega)]\\&+v_q^2(1-e^{-2qd})[\Pi_1(q,\omega)\Pi_2(q,\omega)+\Pi_2(q,\omega)\Pi_3(q,\omega)]\\&+v_q^2(1-e^{-4qd})[\Pi_1(q,\omega)\Pi_3(q,\omega)]\\&-v_q^3(1-2e^{-2qd}+e^{-4qd})[\Pi_1(q,\omega)\Pi_2(q,\omega)\Pi_3(q,\omega)]\end{aligned} \tag{3}$$

For the case of monolayer (double layer), $\Pi_2(q,\omega)=\Pi_3(q,\omega)=0$ ($\Pi_3(q,\omega)=0$). v_q term indicates the intra-layer contribution. ${v_q}^2$ and ${v_q}^3$ terms indicate the contribution from the coupling between the adjacent layers.

The contributions to the optical conductivity are from electron-hole excitations from the intra-layer and inter-layers. In each layer, there are two transition channels (intra- and inter-band transitions) contributing to the optical absorption. When the applied optical field is present, the carriers are excited from the occupied states to the unoccupied states. The intra-band contribution corresponds to electron excitation in the vicinity of the Fermi level within the conduction band. While the inter-band contribution corresponds to the carrier excitation from the valence band to the conduction band and has a turning point at $2E_F$. These two processes are intra-layer case given by the v_q term in Eq. (3). The inter-layer contributions are given by the other v_q^2, v_q^3 terms.

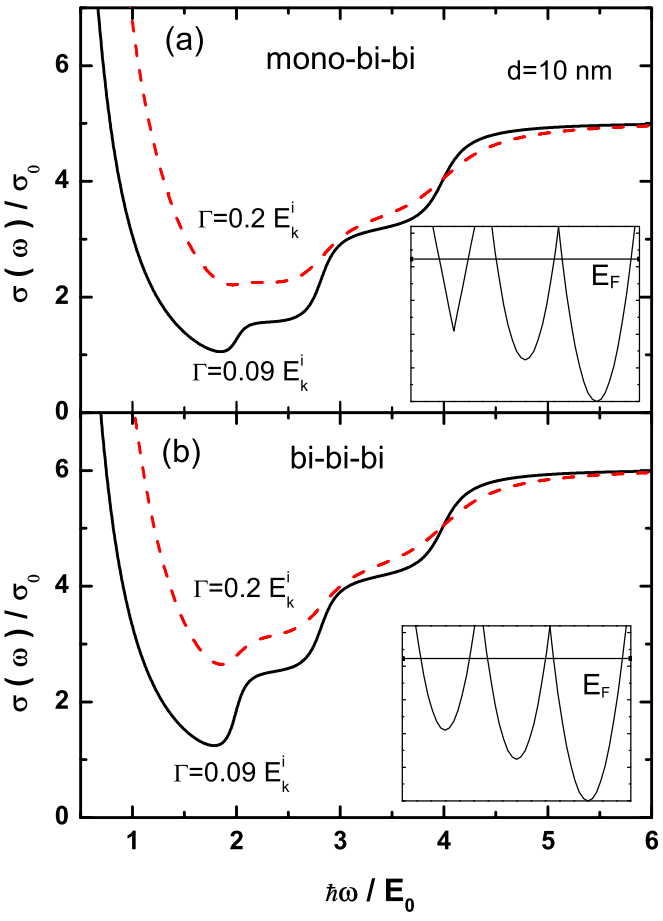

Fig. 3. The optical conductivity as a function of photon energy for two kinds of layer structures. The parameters are same as Fig. 1(a) expect increasing the broadening width to $\Gamma_i = 0.2E_k^i$.

3. Results and discussions

In this paper, we present the analytical and numerical results for the optical conductivity in a three layer graphene system at a low-temperature limit $T \to 0$ K. We take the typical sample parameters in the calculation. The electron density $n_e \sim 10^{12}$ cm^{-2} has been found experimentally which can be tuned by the gate voltage. In our calculation, the Fermi energy E_0 with the electron density $n_{e0}=10^{12}$ cm^{-2} in monolayer graphene was taken as a reference energy throughout the paper. The optical conductivity is an analytical result in a long wavelength limit (i.e., $q \to 0$). The small $q = 0.001k_0$ was taken. The wavevector $k_0 = \sqrt{4\pi n_{e0}/g_s g_v}$.

Fig. 1 shows the schematic of the energy structure for three layer graphene system. The electron density in a different layer is different. At the Fermi energy, the kinetic energy $E_k{}^i$ is different for different layer. In a each separate layer, it could be the mono- or bilayer graphene. $n_{e1} = n_{e0}$, $n_{e2} = 2n_{e0}$, $n_{e3} = 4n_{e0}$ are taken for each monolayer graphene in our numerical calculation. The density of states $D(E) = g_s g_v E/2\pi(\hbar v_F)^2$, $g_s g_v m/2\pi\hbar^2$ for mono- and bilayer graphene respectively. Replacing the monolayer with the bilayer graphene, the density of states increase with more electron densities occupied. Therefore, the electron densities increase to $n_{e1} = 2.9n_{e0}$, $n_{e2} = 4.1n_{e0}$, $n_{e3} = 5.8n_{e0}$ for each bilayer graphene with the very close Fermi energy as the monolayer case in our calculation.

Fig. 2 shows the numerical optical conductivity results with different layer structure. The potential difference between the layers make the different electron density n_{ei} in a distinct layer, which induces the different Fermi wavevector $k_F{}^i$ and the different kinetic energy $E_k{}^i$ at the Fermi energy in each layer. $\Gamma_i = 0.09E_k^i$ is assumed for the broadening widths. From Fig. 2, it can be seen clearly that the number of turning points relates to the layer number. The magnitude of the optical conductivity at the turning point depends on the type of the layer, such as monolayer graphene or bilayer graphene. Each threshold structures are observed at $2E_k^i$, which originates from the occupied valence band to unoccupied conduction band (inter-band) transition. These threshold points can be tuned by the gate voltage (or the electron density) [23]. The contribution from this inter-band transition channel is significant and to be a constant when the photon energy is larger than $2E_k^i$. From the turning curves, the layer number, the layer structure, the electron density, and the Fermi wavevector can be obtained. In the low energy region, only the intra-band transition occurs and the optical conductivity is increasing with decreasing the radiation field which is consistent with the experiment results [23]. When the optical energy is greater than $2E_F$, the optical conductivity is an integer multiple of $\sigma_0 = \frac{e^2}{4\hbar}$. From our numerical calculation, there is weak dependence on the distance between the adjacent layers which can be understood from Eq. (3). The contribution from the interlayer coupling relates to the distance "d" and depends on the factor, such as, $(1 - e^{-2qd})$ and the real part of the d–d correlated function. In the small $-q$ limit ($q \to 0$), the $(1 - e^{-2qd})$ factor and $\mathrm{Re}\Pi(\omega,\mathrm{q})$ are small. Therefore, changing the distance "d" has no obvious influence on the optical conductivity.

The width of the optical absorption at low temperature is determined by disorder. Scattering on impurities is believed to be the most important scattering mechanism determining the energy broadening at low temperature [28,40]. In the present paper, a finite value of broadening width was assumed simply. Increasing the broadening Γ_i, the broadening of the threshold of the inter-band transition at $2E_k^i$ in the optical conductivity spectrum is more gradual as shown in Fig. 3. Therefore, in the intermediate energy region, the strength of the disorder shows a clear influence on the optical conductivity qualitatively. When the optical energy larger than $2E_F$, there is no obvious influence on the optical conductivity. In a low energy region, the magnitude of $\sigma(q, \omega)$ enlarges as the broadening width increasing.

Fig. 4(a) shows the optical conductivity as a function of the photon energy at different static dielectric constant κ, which indicates graphene immersed in different dielectric environments. Here, the layer structure is a mono-bi-bi graphene system. The numerical results indicate that the main influence on the optical conductivity induced by the static dielectric constant is in low energy region (far infrared energy region). Decreasing the static dielectric constant κ, the obvious influence has been obtained and the magnitude of the optical conductivity is lower than the unscreened value. When the optical incident frequency ω decreasing to 0, $\mathrm{Im}\Pi_{L,i}^{+,+}(q, \omega)$ increasing and the optical conductivity continues to increase. In Ref. [33], the optical conductivity of multilayer graphene was investigated. The multilayer Hamiltonian has been decomposed effectively into independent parts in subsystems of bilayer or monolayer graphene. For the bilayer subsystem, the effective interlayer hopping strength γ_m is related to the layer number m which is different from the bilayer graphene system. Therefore, there is an extra label m in the four eigenvalues which providing the possible transition channels and corresponding to several peak structures in the infrared region. In our work, the coupling between the adjacent layer is included which is independent of the layer number and only one peak structure is observed in the infrared region. But our interlayer coupling is related to the dielectric environment which affects the value of the optical conductivity. This properties can be seen in Fig. 3 of Ref. [14]. Fig. 4(b)–(d) show the real and imaginary parts and the

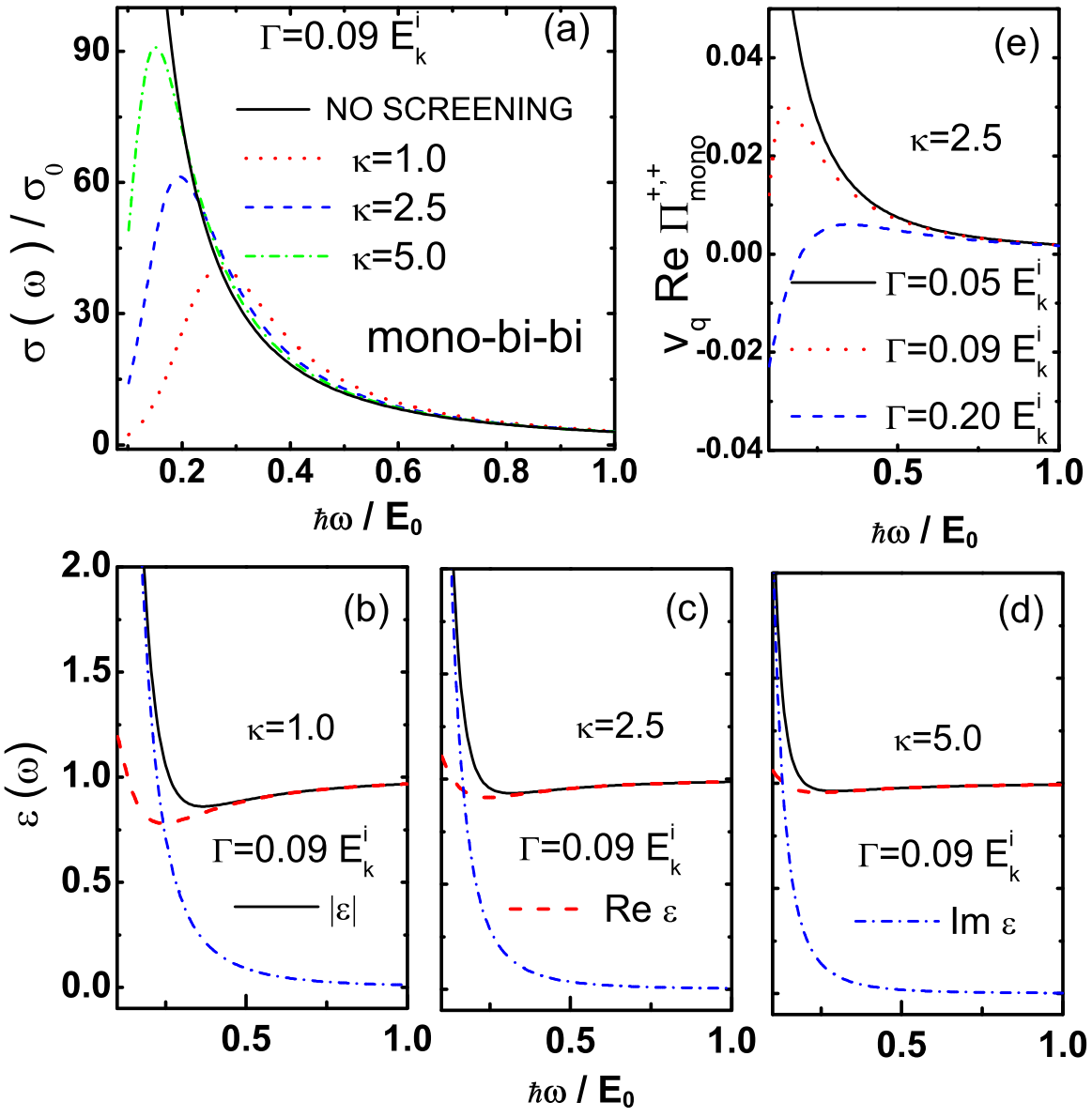

Fig. 4. The optical conductivity as a function of photon energy at different static dielectric constant κ for graphene (a). (b)–(d) indicate the corresponding real, imaginary parts and determination of the dielectric function. The real part of the d–d correlation function at different broadening width for monolayer graphene (e). $d=10$ nm.

determination of the dielectric function at the corresponding static dielectric constant of Fig. 4(a). The main contribution of imaginary part and the main influence of the real part of the dielectric function occurs when the photo energy is compared with the broadening width and depends on the static dielectric constant. When the broadening width $\Gamma \to 0$, the plasmon was obtained in the low frequency region in several graphene systems [20–22,35,36,41]. In the presence of a finite broadening width, the carriers have been scattered by the disorder which destroys the plasmon state. Fig. 4(e) shows the real part of the d–d correlation function at different broadening width for monolayer graphene. The dielectric screening function depends on the wavevector, the broadening width, the optical energy, and the static dielectric constant. In the optical transition process, the change of the wavevector of the electrons $q \to 0$. Increasing the broadening width, the obvious influence on the real part of d–d correlation function in the low optical energy region can be obtained.

In summary, the longitudinal optical conductivity in three layer graphene systems has been investigated. In each layer, it would be monolayer or bilayer graphene. The dependence of the optical conductivity as a function of photon energy on the electron densities, the layer structure, broadening width, dielectric environment is shown in Figs. 2–4. The potential function is created between the layers. The carrier density in each layer is assumed to be tuned by the gate voltage, respectively. From the analytical and numerical results, the following results can be obtained. (I) There are intra-layer and inter-layer contributions to the optical conductivity. The intra-layer part includes the intra-band (given by the term with $++$) and inter-band (given by the terms with $-+$) transitions channels in each layer. (II) The inter-band transition turns on at $2E_k^i$ which can be tuned the position by the gate voltage. When the optical energy close to $2E_k^i$, the optical conductivity exhibits a threshold structure. The mono- or bilayer graphene can be obtained from the ratio of $\sigma(\omega)/\sigma_0$ in each layer, and the corresponding carrier density and the Fermi wavevector can be obtained. The number of the onset depends on the number of layers with different electron density. Actually, the device applications based on graphene material require an intended thickness. For this purpose, using the optical conductivity measure method, the number of layers can be obtained. Other measurements, such as,

the quantized oscillations of electron reflectivity using low-energy electron microscopy [42], the Raman spectrum [43], transmittance of white light [44] are used to obtain the number of layers. (III) The intra-band transition process gives the main contribution in the low photo energy region. (IV) The inter- and intra-layer contribution relates to the coupling between the adjacent layers. Our calculation results show that the dependence of the optical conductivity on the distance d is very weak. (V) The broadening width relates to the scattering mechanism. Different manipulated methods to obtain graphene systems, the disorder is different. Increasing the broadening width, the optical conductivity mutation induced by the inter-band transition is more gradual and the intra-band contribution is increasing. (VI) In the low optical energy region, the static background dielectric environment and the broadening width exhibit an obvious influence on the optical conductivity from the intra-band transition channel via the dielectric screening.

Acknowledgments

This work was supported by the Natural Science Foundation of Jiangsu Province (BK20131428), the Scientific Research Foundation for the Returned Overseas Chinese Scholars from State Education Ministry of China and the Qing-Lan Project of Jiangsu Province (Yang). The National Natural Science Foundation of China (11547030). Z. Ao acknowledges the financial supports from the Chancellor's Research Fellowship program of the University of Technology Sydney.

References

[1] K.S. Novoselov, A.K. Geim, S.V. Morozov, D. Jiang, M.I. Katsnelson, I. V. Grigorieva, S.V. Dubonos, A.A. Firsov, Nature 438 (2005) 197–200.
[2] M.I. Katsnelson, K.S. Novoselov, A.K. Geim, Nature 2 (2006) 620–625.
[3] S.V. Morozov, K.S. Novoselov, M.I. Katsnelson, F. Schedin, D.C. Elias, J. A. Jaszczak, A.K. Geim, Phys. Rev. Lett. 100 (2008) 016602.
[4] Seyong Kim, Insun Jo, Junghyo Nah, Z. Yao, S.K. Banerjee, E. Tutuc, Phys. Rev. B 83 (2011) 161401.
[5] H. Schmidt, T. Lüdtke, P. Barthold, E. McCann, V.I. Falko, R.J. Haug, Appl. Phys. Lett. 93 (2008) 172108.
[6] Tsuneya Ando, Mikito Koshino, J. Phys. Soc. Jpn. 78 (10) (2009) 104716.
[7] Andrea F. Young, Philip Kim, Nat. Phys. 5 (2009) 222–226.
[8] J. Velasco Jr, Y. Lee, L. Jiang, G. Liu, W. Bao, C.N. Lau, Solid State Commun. 152 (2012) 1301–1305.
[9] N. Stander, B. Huard, D. Goldhabr-Gordon, Phys. Rev. Lett. 102 (2009) 026807.
[10] T. Ando, Y. Zheng, H. Suzuura, J. Phys. Soc. Jpn. 71 (2002) 1318–1324.
[11] E.H. Hwang, S. Das Sarma, Phys. Rev. B 79 (2009) 165404.
[12] A. Deshpande, B.J. Leroy, W. Bao, Z. Zhao, C.N. Lau, Appl. Phys. Lett. 95 (2009) 243502.
[13] C.N. Lau, W. Bao, J.V. Jr, Materialstoday, vol. 15, 2012, pp. 238–245.
[14] I. Khrapach, F. Withers, T.H. Bointon, D.K. Polyushkin, W.L. Barnes, S. Russo, M. F. Craciun, Adv. Mater. 24 (2012) 2844–2849.
[15] W.Z. Bao, J.Y. Wan, X.G. Han, X.H. Cai, H.L. Zhu, Dohun Kim, D.K. Ma, Y.L. Xu, Jeremy N. Munday, H. Dennis Drew, Michael S. Fuhrer, L.B. Hu, Nat. Commun. 5 (2014) 4224.
[16] (a) E.H. Hwang, S. Das Sarma, Phys. Rev. B 78 (2008) 075430; (b) W.K. Tse, S.Das Sarma, Phys. Rev. B 75 (2007) 045333.
[17] Wang-Kong Tse, Ben Yu-Kuang Hu, S. Das Sarma, Phys. Rev. B 76 (2007) 081401.
[18] I.V. Gornyi, A.D. Mirlin, F. von Oppen, Phys. Rev. B 70 (2004) 245302.
[19] Hongki Min, E.H. Hwang, S. Das Sarma, Phys. Rev. B 86 (2012) 081402.
[20] E.H. Hwang, S. Das sarma, Phys. Rev. B 80 (2009) 205405.
[21] S. Das Sarma, Qiuzi Li, Phys. Rev. B 87 (2013) 235418.
[22] S. Das Sarma, E.H. Hwang, Phys. Rev. Lett. 102 (2009) 206412.
[23] Z.Q. Li, E.A. Henriksen, Z. Jiang, Z. Hao, M.C. Martin, P. Kim, H.L. Stormer, D. N. Basov, Nat. Phys. 4 (2008) 532.
[24] K.F. Mak, M.Y. Sfeir, Yang Wu, C.H. Lui, James A. Misewich, Tony F. Heinz, Phys. Rev. Lett. 101 (2008) 196405.
[25] A.B. Kuzmenko, E. van Heumen, F. Carbone, D. van der Marel, Phys. Rev. Lett. 100 (2008) 117401.
[26] T. Stauber, N.M.R. Peres, A.K. Geim, Phys. Rev. B 78 (2008) 085432.
[27] Adolfo G. Grushin, Belén Valenzuela, María A.H. Vozmediano, Phys. Rev. B 80 (2008) 155417.
[28] C.H. Yang, F.M. Peeters, W. Xu, Phys. Rev. B 82 (2010) 205428.
[29] D.S.L. Abergel, Vladimir I. Fal'ko, Phys. Rev. B 75 (2007) 155430.
[30] E.G. Mishchenko, Phys. Rev. Lett. 98 (2007) 216801.
[31] Hongki Min, A.H. MacDonald, Phys. Rev. Lett. 103 (2009) 067402.
[32] Y.M. Xiao, W. Xu, F.M. Peeters, Opt. Commun. 328 (2014) 135.
[33] Lei Hao, L. Sheng, Solid State Commun. 149 (2009) 1962.
[34] S. Das Sarma, A. Madhukar, Phys. Rev. B 23 (1981) 805.
[35] E.H. Hwang, S. Das Sarma, Phys. Rev. B 75 (2007) 205418.
[36] Rajdeep Sensarma, E.H. Hwang, S. Das Sarma, Phys. Rev. B 82 (2010) 195428.
[37] E.H. Hwang, S. Das Sarma, Phys. Rev. Lett. 101 (2008) 156802.
[38] E.G. Mishchenko, B.I. Halperin, Phys. Rev. B 68 (4) (2003) 045317.
[39] C.H. Yang, W. Xu, Z. Zeng, F. Lu, C. Zhang, Phys. Rev. B 74 (2006) 075321.
[40] C.H. Yang, F.M. Peeters, W. Xu, Phys. Rev. B 82 (2010) 075401.
[41] X.F. Wang, T. Chakraborty, Phys. Rev. B 75 (2007) 041404.
[42] H. Hibino, S. Mizuno, H. Kageshima, M. Nagase, H. Yamaguchi, Phys. Rev. B, vol. 80, 2009, p. 085406 and references (9–11) therein.
[43] I. Calizo, I. Bejenari, M. Rahman, G. Liu, A.A. Balandin, J. Appl. Phys. 106 (2009) 043509.
[44] R.R. Nair, P. Blake, A.N. Grigorenko, K.S. Novoselov, T.J. Booth, T. Stauber, N.M. R. Peres, A.K. Geim, Science 320 (2008) 1308.